SIZE DEPENDENT EFFECTS

H$_3$PW$_{12}$O$_{40}$ supported on mesoporous MCM-41 and Al–MCM-41 materials: preparation and characterisation

E. Kraleva · M. L. Saladino · A. Spinella ·
G. Nasillo · E. Caponetti

Abstract MCM-41 and Al–MCM-41 has been synthe-sized using cetyl-trimethylammonium bromide (CTAB) surfactant as template and adding the silica precursor to aqueous solutions containing CTAB. The obtained solids were calcined at 600 °C for 4 h. HPW heteropolyacid supported on the mesoporous were prepared using the incipient wetness method. The characterization of materi-als was performed by X-ray diffraction, Transmission Electron Microscopy, N$_2$ adsorption, ^{29}Si Cross Polariza-tion–Magic Angle Spinning and ^{27}Al MAS NMR. Results showed that the hexagonal structure is obtained in both cases. The Aluminium species are located inside an extra-framework. The impregnation reduces the surface area of the mesoporous materials especially of the Al–MCM-41 suggesting a participation of aluminium during the impregnation. HPW is well dispersed in the mesoporous materials and is located inside the pores interacting with the silanol group of the pores wall. ^{27}Al MAS NMR measurements have showed that the impregnation causes the removal of the non-framework aluminium.

E. Kraleva (✉)
Institute of Biodiversity and Ecosystems Research, Bulgarian Academy of Sciences, Sofia, Bulgaria
e-mail: ekraleva@gmail.com

M. L. Saladino · E. Caponetti
Dipartimento di Chimica "S. Cannizzaro", Università di Palermo and INSTM-Udr Palermo, Parco d'Orleans II Viale delle Scienze pad 17, 90128 Palermo, Italy

A. Spinella · G. Nasillo · E. Caponetti
Centro Grandi Apparecchiature—UniNetLab, Università di Palermo, Via F. Marini 14, 90128 Palermo, Italy

Introduction

During the past decade, mesoporous materials of the M41S (Mobil Composition of Matter) family have attracted worldwide attention [1]. These materials have unique properties, such as high specific surface area and pore volume, tuneable pore size and narrow pore size distribu-tion. All these features can be useful in many applications such as catalysis, photocatalysis, adsorption, gas separation and ion exchange. Among the members of this class of materials, those known as MCM-41 have been most widely studied, mainly because of its pseudo-crystalline and tex-tural properties, such as the hexagonal arrangement of one-dimensional channels, mean pore diameters in the range of 20–100°Å and high surface areas (>1000 m^2/g) [2].

In general, the structural and textural characteristics of such molecular sieves are directly related to the synthesis conditions: the type of surfactant, pH, presence of elec-trolytes, temperature, solvents and ageing/preparation time [3–7]. On the other hand, the incorporation of heteroatoms in the MCM-41 structure, transition metals or Al has recently gained considerable interest because it promotes the appearance of active catalytic sites (acid or redox) which may suit them for applications in heterogeneous catalysis such as hydrocarbon catalytic cracking [8, 9], isomerization [10, 11], hydrodesulphurization [12, 13], oxidation reactions, hydroxylation and epoxidation of aromatics, olefins and phenols [14–19].

The acidity of Si–MCM-41 can be increased introducing some strong acid species like sulphate ions [20], sulphated zirconia [21] or heteropolyacids with Keggin structure [22, 23].

Tarafdar et al. [24] reported a sol–gel method in basic conditions using inexpensive zirconia and silica sources to obtain a mesocomposite with high zirconia content

showing both Lewis and Bronsted acidity. However, these mesocomposites have a low porosity, less than 0.4 mL/g. Chen et al. [25], doping Si–MCM-41 with Zr^{4+} into the framework and with sulphate in the surface, have obtained a long-range ordered Zr–MCM-41 mesostructure with enhanced thermal stability, surface area larger than 600 m^2/g and pore volume higher than 0.7 mL/g; unfortunately, the Bronsted acidity of the resultant solids was not noticeably promoted.

Al–MCM-41 mesoporous silica has been used as adsorbent for the removal of oxalic acid from aqueous solution [26] and to incorporate metals by direct inclusion of various precursors to use as catalyst in electrochemical devices [27]. Carriazo et al. [28] have prepared heteropolyacids supported on MCM-41 silica to study the adsorption of 2-butanol. Wang et al. [29–31] have studied the Al–MCM-41 grafted with 12-tungstophosporic acid producing heteropolycompound/Al–MCM-41 hybrid catalysts containing a great number of Bronsted acid sites with strong acid strength.

The aim of this study is to investigate the modifications of the framework of MCM-41 by incorporation in situ of Al^{3+} ions and of the surface depositing $H_3PW_{12}O_{40}$ heteropolyacid (referred as HPW) in order to obtain a supported catalyst. The preparation of MCM-41 and of Al–MCM-41 has been performed using sol–gel method. The HPW/MCM-41 materials have been prepared using the impregnation method. A detailed characterization of the materials was made using X-ray diffraction (XRD), Transmission Electron Microscopy (TEM) equipped with EDS detector, N_2 adsorption–desorption isotherms, ^{29}Si Cross Polarization–Magic Angle Spinning and ^{27}Al Magic Angle Spinning NMR (^{29}Si CP–MAS NMR and ^{27}Al MAS NMR).

Experimental

Materials

Tetraethoxysilane (TEOS, Fluka) and aluminium tri-sec-butoxide (Aldrich) were the sources of Si^{4+} and Al^{3+} ions, respectively. Cetyltrimetylammonium bromide (CTAB, Aldrich), ammonia solution (Aldrich, 28%), ethanol (Fluka) and $H_3PW_{12}O_{40}$ (HPW, Aldrich) were used as received. Solutions were prepared by weight adding conductivity grade water.

Synthesis of mesoporous materials

The MCM-41 and of Al–MCM-41 were prepared using CTAB surfactant as template. CTAB, ethanol, ammonia and water were mixed together and the mixture was stirred from 20 to 45 min. Silica precursor (tetraethyl orthosilicate, TEOS) was added to basic aqueous solutions. Components of the mixture were in molar ratio:

TEOS = 1　CTAB = 0.6　NH_4OH = 12.5

ethanol = 40　H_2O = 174

The introduction of aluminium was performed during the synthesis ''in situ'' just before NH_4OH was added in the Al/Si molar ratio equal to 25.

Synthesis of HPW/MCM-41 catalysts

The supported catalysts were prepared by impregnation of HPW following the procedure of Kozhevnikov et al. [32]. Typically, 1 g of MCM-41 was suspended in 20 mL of HPW aqueous solution, thus loadings of 20 wt%. After stirring the suspension at room temperature for 24 h, the solvent was evaporated. The materials were dried at 120 °C for 4 h and calcined at 400 °C for 4 h.

Characterization techniques

X-ray powder diffraction patterns were recorded in the 20–140° 2θ range at steps of 0.03° and counting time of 3 s/step on a Philips PW 1050 diffractometer, equipped with a Cu tube and scintillation detector beam. The X-ray generator worked at 40 kV and 30 mA. The instrument resolution (divergent and antiscatter slits of 0.5°) was determined using standards free from the effect of reduced crystallite size and lattice defects.

Nitrogen adsorption–desorption isotherms were registered at 77 K using a Quantachrome Nova 2200 Multi-Station High Speed Gas Sorption Analyzer. Samples were outgassed for 3 h at 573 K in the degas station. Adsorbed nitrogen volumes were normalized to standard temperature and pressure. The specific surface area (S_{BET}) was calculated according to the standard BET method [33] in the relative adsorption pressure (P/P_0) range from 0.045 to 0.250. The total pore volume (V_t) was obtained from the nitrogen amount adsorbed in correspondence of P/P_0 equal to 0.99. The cylinder diameter size (w_{BJH}) was calculated by the BJH method [34]. The pore wall thickness (t) was then estimated using the equation:

$$t = a_0 - kw \tag{1}$$

where k is a constant that for hexagonal cylinder and pore wall mass density was obtained by using geometrical consideration equal to 0.95 [35].

Transmission Electron Microscopy study was performed using a JEM-2100 (JEOL, Japan) operating at 200 kV accelerating voltage, equipped with an energy dispersive X-ray spectrometer (EDS) (Oxford, UK) suited for element

identification. The powder in isopropanol was sonicated to ensure a homogeneous dispersion. A small drop was deposited on a 200 mesh carbon-coated copper grid, which was introduced into the TEM chamber analysis after complete solvent evaporation.

^{29}Si Cross Polarization–Magic Angle Spinning Nuclear Magnetic Resonance (^{29}Si {^{1}H} CP–MAS NMR) spectra were obtained at room temperature by means of a Bruker Avance II 400 MHz (9.4 T) spectrometer operating at 79.4 MHz for ^{29}Si nucleus with a MAS rate of 5 kHz, 4096 scans, contact time of 8 ms and repetition delay of 8 s. A contact time of 8 ms was optimized on the samples through variable contact time experiments and the optimization of the Hartmann-Hanh condition [36] was obtained by means of a Q8M8 (Si[(CH$_3$)$_3$]$_8$Si$_8$O$_{20}$) standard. Samples were compressed in 4 mm zirconia rotors with Kel-F (PCTFE) caps.

^{27}Al MAS NMR spectra were obtained at room temperature by means of a Bruker Avance II 400 MHz (9.4 T) spectrometer operating at 104.26 MHz for ^{27}Al nucleus with a MAS rate of 13 kHz, 200 scans, a pulse of 5 μs on the ^{27}Al nucleus and a repetition delay of 2 s. Samples were compressed in 4 mm zirconia rotors with Kel-F (PCTFE) caps.

Results and discussion

XRD diffraction patterns of MCM-41 and of Al–MCM-41 materials are reported in Fig. 1.

The XRD patterns of MCM-41 materials showed tree characteristic peaks that can be indexed as (100), (110) and (200) reflections of hexagonal lattice of a typical MCM-41. The Al–MCM-41 show a better resolution of the 110 and 200 reflections indicating a higher hexagonal order of mesopores, and then a material with better structure stability.

XRD diffraction patterns of HPW/MCM-41 and HPW/Al–MCM-41 materials are reported in Fig. 1. The diffraction patterns still show the three peaks of the supports, even if with lower intensity, indicating that the samples maintain the hexagonal lattice symmetry. The reduction in the intensity is probably due to the nanosize of the impregnated particles present in the pores [18]. Reflections of HPW phases are not observed in the high angle region of XRD patterns, suggesting that they are well dispersed or amorphous [28, 37].

d_{100} spacing, corresponding to the plane distance, was computed using the Bragg's law. In the hexagonal structure, it is correlated with the adjacent pores centre-centre distance a_0 using the following equation [38]:

$$a_0 = 2d_{100}/\sqrt{3} \tag{2}$$

The obtained a_0 values are reported in Table 1.

Results show that the aluminium presence causes an increase of the adjacent pores centre–centre distance. Interplanar distance modification observed in the impregnated samples supports the hypothesis of introduction of HPW species into to the silica network.

TEM micrographs of MCM-41 and HPW/MCM-41 samples are reported in Fig. 2.

TEM analysis shows MCM-41 nanoparticles (after the calcinations at 600 °C for 4 h) having sizes of about 200–300 nm. After impregnation, TEM measurements confirm the absence of structural collapse of MCM-41 during impregnation and that the nanoparticles assemble themselves in bigger aggregates maintaining the original dimensions. In HPW/MCM-41, the inner structure is well preserved: the original channels of MCM-41 can be observed in the right micrograph of Fig. 2. It supports the idea that the HPW is well dispersed.

EDS analysis, reported in Fig. 3, carried out in the area drawn by dots of Fig. 2 shows the peaks of W, Si and O
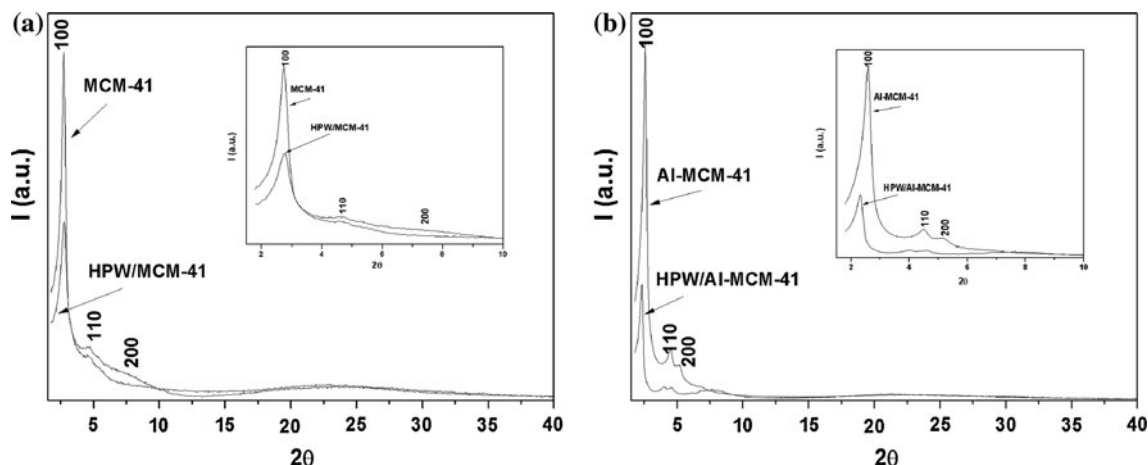

Fig. 1 XRD patterns of a MCM-41 and HPW/MCM-41; b Al–MCM-41 and HPW/Al–MCM-41 samples

Table 1 Structural data obtained from the XRD pattern and from isotherm analysis

Sample	α_0 (Å)	S_{BET} $(m^2 g^{-1})*$	w_{BJH} (Å)	V_t (cc/g)	t (Å)
MCM-41	37(1)	931(46)	24	0.76	13
HPW/MCM-41	37(1)	845(42)	21	0.46	16
Al–MCM-41	40(1)	1123(56)	30	0.84	10
HPW/Al–MCM-41	43(1)	50(2)	37	0.12	6

together with Cu of grid indicating the presence of the heteropolyacid in the sample.

The N_2 adsorption–desorption isotherms of samples are reported in Fig. 4.

According to the IUPAC classification [39], they correspond to type IV, typical of mesoporous materials. Three well-defined regions may be identified: (1) a slow increase in nitrogen uptake at low relative pressure, corresponding to a monolayer–multilayer adsorption on the pore walls; (2) a sharp step at intermediate relative pressures indicative of a capillary condensation within mesopores and (3) a plateau with a slight inclination at high relative pressure associated with multilayer adsorption on the external surface of the materials [39]. The capillary condensation of nitrogen inside the mesopores occurs in the P/P_0 range 0.3–0.4 in all cases. It is worthy to note that the isotherm of HPW/Al–MCM-41 sample is different from the others indicating a lower interaction between the adsorbate and the absorbent. This could be due to the lock of the pores from the heteropolyacid and suggest that the Al–MCM-41 support better promote the impregnation process than the MCM-41.

The specific surface area (S_{BET}), the total pore volume (V_t), the cylinder diameter size (w_{BJH}) and the pore wall thickness (t) values are reported in Table 1.

High surface area values were observed. The aluminium incorporation causes an increase of surface area. Surface

Fig. 3 EDS spectrum of HPW/MCM-41 sample carried out in the area drawn by *dots* of Fig. 2

area of MCM-41 material decreased with the impregnation, and a significantly change can be observed in the HPW/Al–MCM-41. As a consequence, V_t and w decrease, while t values increase.

The ^{29}Si {^1H} CP–MAS NMR spectra of support and impregnated samples are reported in Fig. 5.

Each ^{29}Si {^1H} CP–MAS NMR spectrum of the Fig. 5 is due to the contribution of three peaks: the first peak, Q2, centred at around −90 ppm, is attributed to the geminal silanols, the second peak, Q3, at around −100 ppm, is attributed to the silicon atoms bearing one hydroxyl group and the third peak, Q4, at around −109 ppm, is attributed to the silicon atoms without hydroxyl groups [40, 41].

A downfield shift of the Q2 and Q3 signals in the functionalized samples spectra can be observed. This could be due to the formation of Si–O–Al and Si–O–W bonds during the impregnation process. The higher downfield shift was observed for the HPW/Al–MCM-41 sample, thus implying that the MCM-41 structure is affected by both W
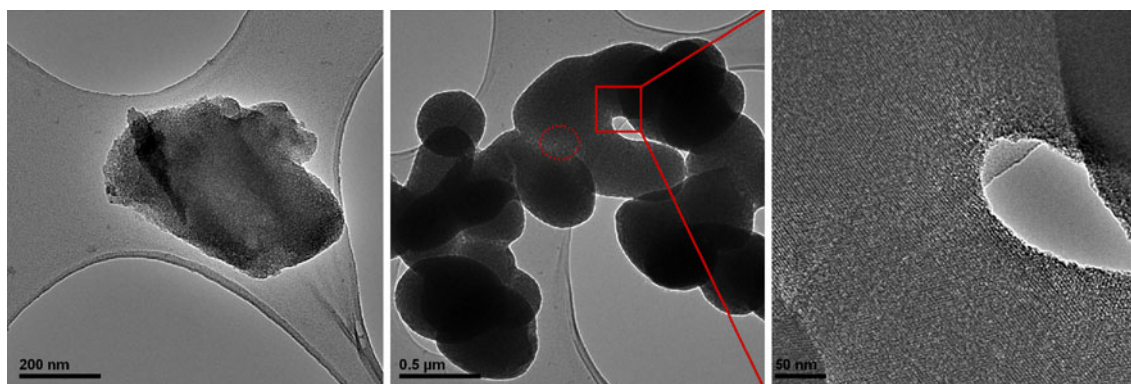

Fig. 2 TEM micrographs of MCM-41 sample (*left*); HPW/MCM-41 sample (*centre*); HPW/MCM-41 sample at higher magnification (*right*)

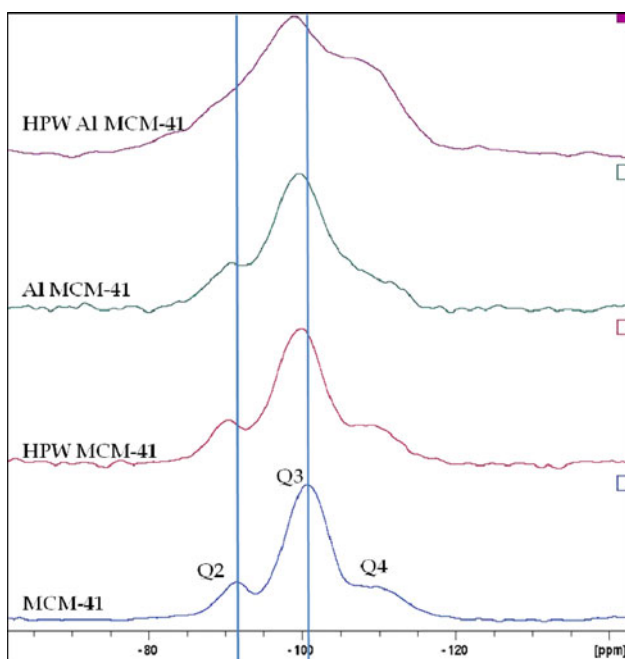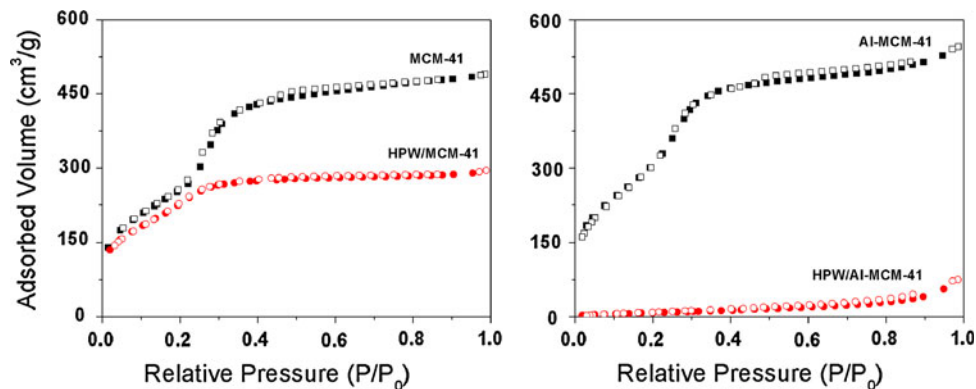**Fig. 4** N₂ adsorption isotherms of samples

Fig. 5 ^{29}Si {^{1}H} CP–MAS NMR spectra of MCM-41, Al–MCM-41, HPW/MCM-41 and of HPW/Al–MCM-41 samples

Fig. 6 Trends of the Qn peak areas for all the samples

and Al ions which are incorporated inside the silica framework.

Furthermore, the spectra of the samples containing Al show very broad signals. This is due to the strong quadripolar interaction between the Al and the Si nuclei which are close to each other in the material framework. Since the ^{29}Si {^{1}H} CP–MAS NMR technique is based on the magnetization transfer from ^{1}H to ^{29}Si nuclei, the peak intensities are related to the total number of protons near the silicon atoms. As a consequence, a straight quantification of the different silicon groups is not possible. However, as the bare and the functionalized MCM-41 spectra show the same the same cross polarization dynamic, the relative intensities of the three different silicon contributions in the three samples are still reliable because the variation of the contact time does not modify
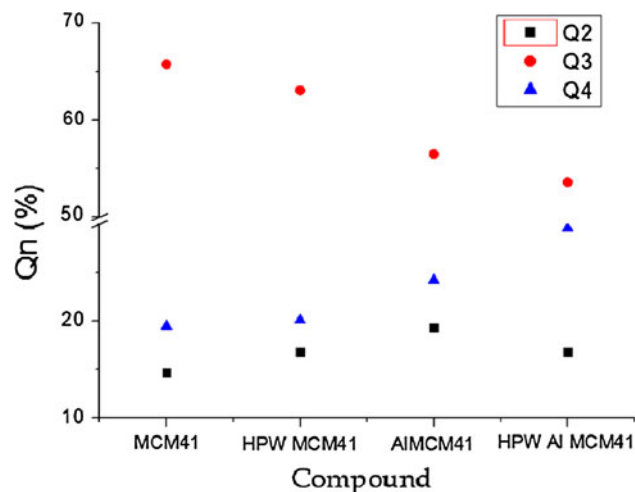
the relative intensity distribution of the signals. Then, the deconvolution of each spectrum has been performed to calculate the single contributions of the three signals.

The relative values of these three NMR signals are reported in Fig. 6.

The trends of the Qn peak areas show a progressive modification of the MCM-41 matrix caused by the presence of the Al and W ions. In particular, the HPW does not greatly affect the areas distribution. On the contrary, a much evident effect is due to the Al ion which causes a decrease of the Q3 and a contemporary increase of the Q2 and Q4 peak areas. This suggests that the Al is in both an extra-framework form interacting with the Si(O–Si)₃OH species and inside the framework. This two aluminium forms cause the increase of the Q4 and the increase of the Q2 species, respectively. This finding is confirmed by the further Al–MCM-41 impregnation with the HPW: the heteropolyacid reacts on the surface with Q2 and Q3 giving rise to Q4 species which are also formed through the calcination process.

The ^{27}Al MAS NMR spectra of Al–MCM-41 and of HPW/Al–MCM-41 are reported in Fig. 7.
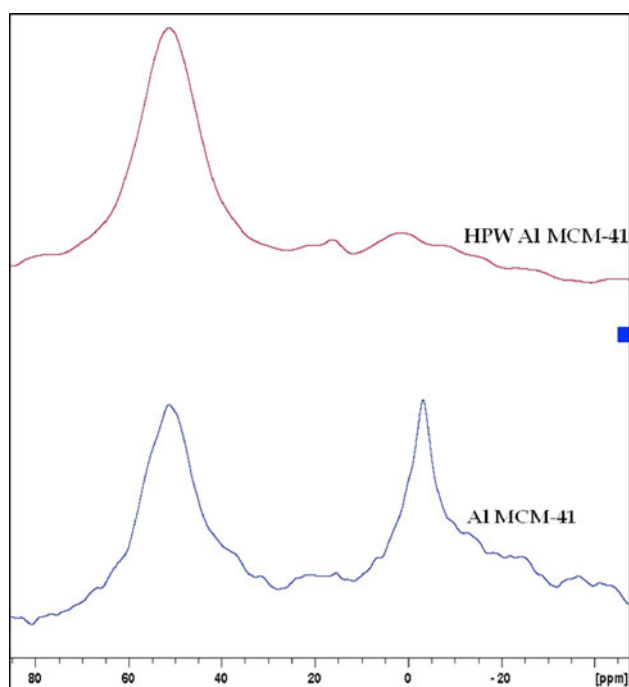
Fig. 7 ^{27}Al {^{1}H} CP–MAS NMR spectra of Al–MCM-41 and of HPW/Al–MCM-41 samples

The ^{27}Al MAS NMR spectrum of the Al–MCM-41 sample shows a resonance peak at around 53 ppm which is attributed to the presence of aluminium in tetrahedral coordination [21, 42] and a peak around 0 ppm due to the non-framework aluminium in octahedral coordination caused by the calcination treatment [43, 44]. The peak at around 0 ppm is not present in the ^{27}Al MAS NMR of the HPW/Al-MCM-41 sample. This is evidence that the impregnation process causes the removal of the non-framework aluminium and that the HPW species are located inside the pores interacting with the silanol group of the pores wall as observed in previous works [45, 46].

Conclusions

The results presented in this article showed that both the introduction of the aluminium species and the heteropolyacid can induce same modification in the mesoporous structure and that the modification can be different depending on the presence of metals inside the framework.

No substantial change in the hexagonal structure has been observed in both cases, but the introduction of aluminium species induces an increase of the adjacent pores centre-centre distance a_0 and of surface area. Aluminium species are located in the extra-framework form interacting with the Si(O–Si)$_3$OH species and inside the framework.

HPW presence causes a decrease of surface area in the MCM-41, especially in the Al–MCM-41 sample. The total

pore volume and the cylinder diameter size decrease, while the pore wall thickness values increase.

The reported findings suggest that the HPW species are located inside the pores interacting with the silanol group of the pores wall and are supported by ^{29}Si {^{1}H} CP–MAS NMR and ^{27}Al MAS NMR measurements which showed that the impregnation process causes the removal of the non-framework aluminium.

References

1. Beck JS, Roth WJ, Leonowicz ME, Kresge CT, Schmitt KD, Chu CTW, Olson DH, Sheppared EW, McCullen SB (1992) J Am Chem Soc 114:10834
2. Kresge CT, Leonowicz WJ, Roth JC, Vartulli JC, Beck JS (1992) Nature 359:710
3. Occelli ML, Biz SJ (2000) J Mol Catal A 151:225
4. Lindlar B, Kogelbauer A, Kooyman PJ, Prins R (2001) Microporous Mesoporous Mater 89:44
5. Davis ME, Chen CY, Burket SL, Li HX (1993) Microporous Mater 2:27
6. Occelli ML, Biz SJ (1998) Catal Rev Sci Eng 40(3):329
7. Selvam P, Badamali S, Sakthivel A (2000) Catal Today 63:291
8. Corma A, Grande MS, Gonzalez-Alfaro V, Orchilles AV (1996) J Catal 159:375
9. Reschetilowski W, Koch H (1998) Microporous Mesoporous Mater 25:127
10. Seo G, Kim NH, Lee YH, Kim JH (2004) Catal Lett 90:145
11. Landau MV, Dafa E, Kaliya ML, Sen T, Herskowitz M (2001) Microporous Mesoporous Mater 49:65
12. Ohtsuka Y, Takahashi Y, Noguchi M, Takashi A, Takasaki S, Tsubouchi N, Wang Y (2004) Catal Today 89:419
13. Klimova T, Calderon M, Ramírez J (2003) Appl Catal A 204:29
14. Gontier S, Tuel A (1996) J Catal 157:124
15. Yonemitsu M, Tanaka Y, Iwamoto M (1998) J Catal 178:207
16. Zhang Q, Wang Y, Ohishi Y, Shishido T, Takehira K (2001) J Catal 202:308
17. Noreña-Franco L, Hernandez-Perez I, Aguilar-Pliego A, Maubert-Franco A (2002) Catal Today 75:189
18. Su BL, Constantin C, Pârvulescu V (2003) J Mol Catal A 202:171
19. Srinivas N, Radha Rani V, Kulkarni SJ, Radha kishan M, Raghavan KV (2001) J Mol Catal A 172:187
20. Okuhara T, Mizuno N, Misono M (2001) Appl Catal A 222:63
21. Biz S, Occelli ML (1998) Catal Rev Sci Eng 40:329
22. Marme F, Couduruer G, Vérdrine JC (1998) Microporous Mesoporous Mater 22:151
23. Dias JA, Caliman E, Dias SCL, Paulo M, de Souza ATCP (2003) Catal Today 85:39
24. Tarafdar A, Panda AB, Pramanik P (2005) Microporous Mesoporous Mater 84:223
25. Salas P, Chen LF, Wang JA, Armendáriz H, Guzman ML, Montoya JA, Acosta DR (2005) Appl Surf Sci 252(4):1123
26. Gokulakrishnan N, Pandurangan A, Somanathan T, Sinha PK (2010) J Porous Mater 17:763

27. Alonso-Lemus I, Verde-Gomez Y, Aguilar-Elguézabal A, Alvarez-Contreras L (2010) J Nanomater 2010:1–7
28. Carriazo D, Domingo C, Martín C, Rives V (2008) J Solid State Chem 181:2046
29. Yang XK, Chen LF, Wang JA, Noreña LE, Novaro O (2009) Catal Today 148(1–2):160
30. Wang JA, Chen LF, Noreña LE, Navarrete J (2009) Appl Catal A 357(2):223
31. Wang JA, Zhou XL, Chen LF, Noreña LE, Yu GX, Li CL (2009) J Mol Catal A 299(1–2):68
32. Kozhevnikov IV, Sinnema A, Jansen RJJ, Pamin K, van Bekkum H (1995) Catal Lett 30:241
33. Brunauer S, Emmett PH, Teller E (1938) J Am Chem Soc 60:309
34. Kruk M, Antchshuk V, Jaroniec M, Sayari A (1999) J Phys Chem B 103:10670
35. Kruk M, Jaroniec M, Sakamoto Y, Terasaki O, Ryoo R, Ko CH (2000) J Phys Chem B 104:292
36. Hartmann SR, Hahn EL (1962) Phys Rev 128:2042
37. Lopez-Salinas E, Hernandez-Cortez JG, Schifter I, Torres-Garcia E, Navarrete J, Gutierrez-Carrillo A, Lopez T, Lottici PP, Bersani D (2000) Appl Catal A 193:215
38. Aguado J, Serrano DP, Escola JM (2000) Microporous Mesoporous Mater 34:43
39. Gregg SJ, Sing KSW (1982) Adsorption, surface area and porosity, 2nd edn. Academic Press, London
40. Luhmer M, Espinose JB, Hommel H, Legrand AP (1996) Magn Reson Imaging 14:911
41. Stakheev AY, Shpiro ES, Apijok J (1993) J Phys Chem 97:5668
42. Kolodziejski W, Corma A, Navarro MT, Perez-Pariente J (1993) Solid State Nucl Magn Reson 2:253
43. Chen CY, Li HX, Davis ME (1993) Microporous Mater 2:17
44. Matsumoto A, Chen H, Tsutsumi K, Grun M, Unger K (1999) Microporous Mesoporous Mater 32:55
45. Saladino ML, Spinella A, Caponetti E, Minoja A (2008) Microporous Mesoporous Mater 113:490
46. Saladino ML, La Parola V, Longo A, Venezia AM, Spinella A, Caponetti E (2010) Eur J Inorg Chem 23:3628